Cone opsin determines the time course of cone photoreceptor degeneration in Leber congenital amaurosis

Tao Zhang[a,1], Ning Zhang[a,1,2], Wolfgang Baehr[a,b,c], and Yingbin Fu[a,b,3]

Departments of [a]Ophthalmology and Visual Sciences, [b]Neurobiology and Anatomy, and [c]Biology, University of Utah, Salt Lake City, UT 84132

Edited* by King-Wai Yau, Johns Hopkins School of Medicine, Baltimore, MD, and approved April 22, 2011 (received for review November 16, 2010)

Mutations in RPE65 or lecithin-retinol acyltransferase (LRAT) disrupt 11-*cis*-retinal recycling and cause Leber congenital amaurosis (LCA), the most severe retinal dystrophy in early childhood. We used *Lrat*$^{-/-}$, a murine model for LCA, to investigate the mechanism of rapid cone degeneration. Although both M and S cone opsins mistrafficked as reported previously, mislocalized M-opsin was degraded whereas mislocalized S-opsin accumulated in *Lrat*$^{-/-}$ cones before the onset of massive ventral/central cone degeneration. As the ventral and central retina express higher levels of S-opsin than the dorsal retina in mice, our results may explain why ventral and central cones degenerate more rapidly than dorsal cones in *Rpe65*$^{-/-}$ and *Lrat*$^{-/-}$ LCA models. In addition, human blue opsin and mouse S-opsin, but not mouse M-opsin or human red/green opsins, aggregated to form cytoplasmic inclusions in transfected cells, which may explain why blue cone function is lost earlier than red/green-cone function in patients with LCA. The aggregation of short-wavelength opsins likely caused rapid cone degenerations through an endoplasmic reticulum stress pathway, as demonstrated in both the *Lrat*$^{-/-}$ retina and transfected cells. Replacing rhodopsin with S-opsin in *Lrat*$^{-/-}$ rods resulted in mislocalization and aggregation of S-opsin in the inner segment and the synaptic region of rods, ER stress, and dramatically accelerated rod degeneration. Our results demonstrate that cone opsins play a major role in determining the degeneration rate of photoreceptors in LCA.

opsin aggregation | long/medium-wavelength opsin | ubiquitination | retinal degeneration

Retinoid isomerase (RPE65) and lecithin-retinol acyltransferase (LRAT) play key roles in recycling 11-*cis*-retinal in the retinal pigment epithelium (RPE). LRAT catalyzes the esterification of all-*trans* retinol (vitamin A) to all-*trans* retinyl esters (1), which are the substrate for RPE65, to produce 11-*cis*-retinol (2–4). Mutations in either gene lead to Leber congenital amaurosis (LCA), an inherited retinal degenerative disease characterized by severe loss of vision in childhood and early degeneration of foveal cones followed by rods (5). Two murine models, *Rpe65*$^{-/-}$ and *Lrat*$^{-/-}$, capture many salient pathologic features of the human condition (6–8). In both models, apo-rhodopsin traffics normally to rod outer segment (ROS) and rod photoreceptors degenerate slowly. In contrast, cone opsin (S-opsin and M-opsin) apoproteins fail to traffic from cone inner segment to the outer segment, and cone photoreceptors in the central/ventral retina degenerate rapidly (8–11). Constitutive activity of the rhodopsin apoprotein likely causes rod degeneration (12). However, the mechanisms responsible for early cone death in both mouse models and human patients are not well understood. Specifically, it is unclear why ventral and central cones in mouse models die much more rapidly than dorsal cones. Similarly, it is unclear why blue cone function is lost early in patients (13). Here, we used the *Lrat*$^{-/-}$ mouse, a model for LCA, to investigate the mechanism for cone photoreceptor degeneration.

Results

Mistrafficking and Accumulation of Cone Opsins in *Lrat*$^{-/-}$ Retina. In the absence of 11-*cis*-retinal, both S and M opsins were mislocalized in the inner segment, cell body, axon, and synaptic pedicle in P18 *Lrat*$^{-/-}$ cones, as shown previously (8, 11) (Fig. 1). Judging from the relative distribution of opsin signals in different compartments of cones, more S-opsin was mislocalized compared with M-opsin (Fig. 1, *Middle*). Specifically, we observed aggregated S-opsin in the inner segment (Fig. 1, *Bottom Right*, white arrows) and the synaptic layer [i.e., outer plexiform layer (OPL)]. In contrast, M-opsin was barely detectable in the inner segment whereas some M-opsin accumulated in the synaptic layer (Fig. 1, *Top Middle*, red arrow). These features were not observed in WT retina (Fig. 1, *Left*).

Expression and Ubiquitination of Cone Opsins in *Lrat*$^{-/-}$ Retina. As immunohistochemistry data suggested that *Lrat*$^{-/-}$ cones accumulated more mislocalized S-opsin than M-opsin (Fig. 1), we proceeded to verify this finding by Western blot at three stages of cone degeneration: (*i*) postnatal day (P) 14, predegeneration (11); (*ii*) P18, early-stage degeneration; (*iii*) and P30, late-stage degeneration. In P14 *Lrat*$^{-/-}$, the protein levels of both M-opsin and S-opsin were similar to those in WT, although their mRNA levels were slightly reduced (Fig. 2 *A* and *B*). However, in P18 *Lrat*$^{-/-}$ retina, the M-opsin protein was markedly reduced (~1.9 times) whereas the S-opsin level remained the same compared with WT (Fig. 2 *A* and *B*). After we normalized the protein levels of cone opsins against their mRNA levels (i.e., protein/mRNA), this ratio almost doubled (~1.9 times) for S-opsin in P18 *Lrat*$^{-/-}$ compared with WT (Fig. 2*C*, *Left*). In contrast, the protein/mRNA ratio of M-opsin in P18 *Lrat*$^{-/-}$ was similar to that in WT. Assuming the protein synthesis for cone opsins is minimally affected in the early stage of *Lrat*$^{-/-}$ cone degeneration, our results suggest that mislocalized S-opsin was more resistant to proteasome degradation than mislocalized M-opsin, consistent with our immunostaining results (Fig. 1). As the ventral and central retina of *Lrat*$^{-/-}$ lost approximately 30% of cones at P18 (Fig. 2*C*, *Right*), the slower clearance of mislocalized S-opsin resulted in more S-opsin per cone in *Lrat*$^{-/-}$ compared with WT.

The accumulation of mislocalized cone opsins in *Lrat*$^{-/-}$ cones had a direct impact on the time course of cone degeneration. When the protein/mRNA ratio was approximately 1.5 for both

Author contributions: Y.F. designed research; T.Z. and N.Z. performed research; W.B. contributed new reagents/analytic tools; T.Z., N.Z., and Y.F. analyzed data; and Y.F. wrote the paper.

The authors declare no conflict of interest.

*This Direct Submission article had a prearranged editor.

[1]T.Z. and N.Z. contributed equally to this work.

[2]Present address: Department of Pharmacology, School of Medicine, Case Western Reserve University, Cleveland, OH 44106.

[3]To whom correspondence should be addressed. E-mail: yingbin.fu@hsc.utah.edu.

This article contains supporting information online at www.pnas.org/lookup/suppl/doi:10.1073/pnas.1017127108/-/DCSupplemental.

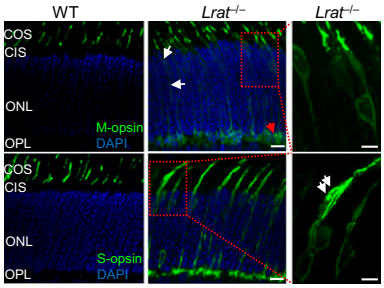

Fig. 1. Mistrafficking and accumulation of cone opsins in P18 *Lrat*$^{-/-}$ retina. *Lrat*$^{-/-}$ and WT retinas were stained with M-opsin and S-opsin antibodies (green). Nuclei were stained with DAPI (blue). In *Lrat*$^{-/-}$ retina, mistrafficking of M-opsin is indicated by white arrows (*Top* and *Middle*). Mistrafficking of S-opsin is apparent. *Right*: Magnified views of two boxed regions from middle. Accumulation and aggregation of S-opsin in the inner segment of an *Lrat*$^{-/-}$ cone is indicated by white arrows. Small amount of aggregated M-opsin is indicated by the red arrow. No immunoreactivity was detected in various mouse retinal sections when control rabbit IgG was used for staining (*SI Appendix*, Fig. S12). COS, cone outer segment; CIS, cone inner segment; ONL, outer nuclear layer. (Scale bars: *Right*, 5 μm; 10 μm elsewhere.)

M and S opsins in P14 *Lrat*$^{-/-}$ retina, there was no cone death in all regions, suggesting cones can tolerate certain amount of mislocalized cone opsins (Fig. 2*C*). However, the increase of this ratio to approximately 1.9 times that of S-opsin accompanied the onset of rapid ventral and central cone degeneration. As the ventral and central retina express higher levels of S-opsin than the dorsal retina in mice (14), our results suggest that accumulation of mislocalized S-opsin may underlie the fast ventral/central cone degeneration in *Lrat*$^{-/-}$. Cones at the far dorsal region, which express more M-opsin than S-opsin, degenerated much more slowly, corresponding to less accumulation of mislocalized M-opsin. In P30 *Lrat*$^{-/-}$, both the protein and mRNA levels of S-opsin were drastically reduced (Fig. 2 *A* and *B*), as a result of significant loss of ventral and central cones (8–11) (Fig. 2*C*, *Right*).

Because proteins with abnormal structure are normally targeted to the ubiquitin–proteasome system (15), and ubiquitination of proteins that aggregate in the neurons of the central nervous system is a key characteristic of neurodegenerative diseases (16), we examined whether S-opsin is ubiquitinated in *Lrat*$^{-/-}$ cones. We performed double labeling with antibodies against cone opsins and ubiquitin on retinas from *Lrat*$^{-/-}$ and *Lrat*$^{+/-}$ [the phenotype of *Lrat*$^{+/-}$ mice was very similar to that of WT mice (7)]. In the ventral retina of P18 *Lrat*$^{-/-}$, aggregated S-opsin colocalized with ubiquitin (Fig. 3*A*, white arrows). In the advanced stage of degeneration at P30, almost all S-opsin colocalized with ubiquitin in the remaining ventral cones of *Lrat*$^{-/-}$ (Fig. 3*B*, white arrows). This increase of S-opsin ubiquitination coinciding with the progress of cone degeneration suggests that S-opsin ubiquitination may contribute to the demise of *Lrat*$^{-/-}$ ventral/central cones. In contrast, the ubiquitin signal was weak in both P18 and P30 dorsal retinas of *Lrat*$^{-/-}$, where more M-opsin was expressed, probably because mislocalized M-opsin was only transiently ubiquitinated before being degraded by the proteasome (Fig. 3 *A* and *B*, *Top*). In control *Lrat*$^{+/-}$ retinas (at P18 and P30), ubiquitin signal was barely detectable (*SI Appendix*, Fig. S1).

Endoplasmic Reticulum Stress in *Lrat*$^{-/-}$ Retina. The accumulation of cone opsins (especially S-opsin) in the endoplasmic reticulum (ER) may activate the unfolded protein response (UPR) and cause ER stress. Persistent ER stress may induce apoptosis in the central/ventral cones. We examined the expression of a B-ZIP transcription factor CHOP (C/EBP homology protein), a UPR

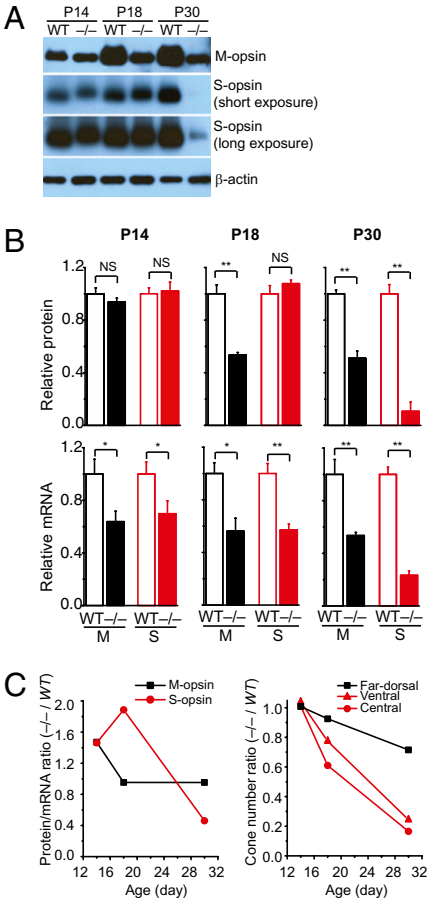

Fig. 2. Expression of M and S opsins in *Lrat*$^{-/-}$ and WT retinas. (*A*) Western blot analysis of M- and S-opsins in the retinas of *Lrat*$^{-/-}$ and WT mice at P14, P18, and P30. Equal loading was indicated by β-actin. (*B*) *Upper*: Protein levels of M and S opsins were quantified from five independent experiments. *Lower*: Normalized mRNA levels of M- and S-opsins. Real-time RT-PCR was performed to quantify the mRNA levels of M- and S-opsins relative to *Gapdh* in P14 (n = 7), P18 (n = 4), and P30 (n = 7) WT and *Lrat*$^{-/-}$ retinas. Values were normalized to WT levels of the respective age for both protein and mRNA comparison. Values represent mean ± SEM and were analyzed by Student t test. *P < 0.05, **P < 0.01, NS, not significant. (*C*) *Left*: Average protein/mRNA ratios of M- and S-opsins of *Lrat*$^{-/-}$ were normalized against those of WT. *Right*: Average cone numbers from ventral, central, and far dorsal retina of *Lrat*$^{-/-}$ were normalized against those of WT.

target gene and an ER stress marker associated with apoptosis (17), in WT and *Lrat*$^{-/-}$ (at P14 and P18) retinas. The CHOP signal was very low in the outer nuclear layer (ONL) of both P14 and P18 WT retinas (Fig. 4 *A* and *B*), consistent with previous work (18). In contrast, the CHOP signal was markedly increased in the ONL of the ventral retina of P18 *Lrat*$^{-/-}$ (Fig. 4*A*, *Bottom Right*), coinciding with the maximal S-opsin accumulation and the early stage of cone degeneration (Fig. 2*C*). The CHOP signal was lower in the ventral retina of P14 *Lrat*$^{-/-}$ when S-opsin accumulation was much less. In the far dorsal retina of *Lrat*$^{-/-}$ (P14 and P18) that mainly expresses M-opsin, no CHOP up-regulation was observed (Fig. 4*B*). Immunolabeling with an isotype control antibody for CHOP did not show nonspecific signals (*SI Appendix*, Fig. S2).

Mouse and Human Short-Wavelength Opsins Were Aggregated and Caused ER Stress in Transfected Cells. We have shown that M-opsin and S-opsin have different aggregation properties under 11-*cis*-retinal deprivation in the mouse retina. We verified this by using

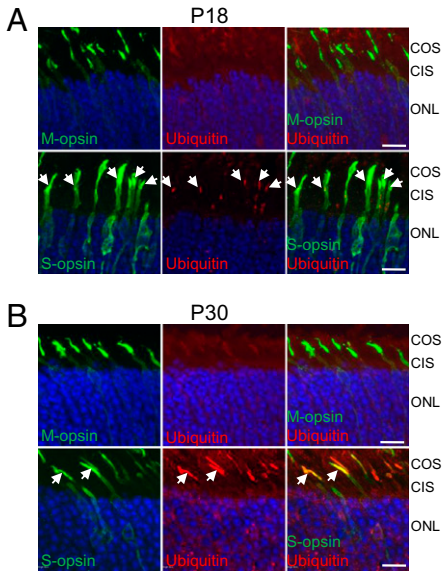

Fig. 3. S-opsin and ubiquitin in *Lrat*$^{-/-}$ cones. (*A*) P18 and (*B*) P30 *Lrat*$^{-/-}$ retinal sections were double-labeled with antibodies against M-opsin or S-opsin (green) and ubiquitin (red). Aggregated S-opsin in P18 *Lrat*$^{-/-}$ cones colocalized with ubiquitin in *A* (white arrows). In P30 *Lrat*$^{-/-}$ retina, extensive colocalization between S-opsin and ubiquitin can be seen (white arrows) in *B*. Nuclei were stained with DAPI (blue). Labeling with isotype control mouse IgG1 (for ubiquitin antibody) or rabbit IgG (for M/S opsin antibodies) did not show nonspecific signals (*SI Appendix*, Fig. S12). (Scale bar: 10 μm.)

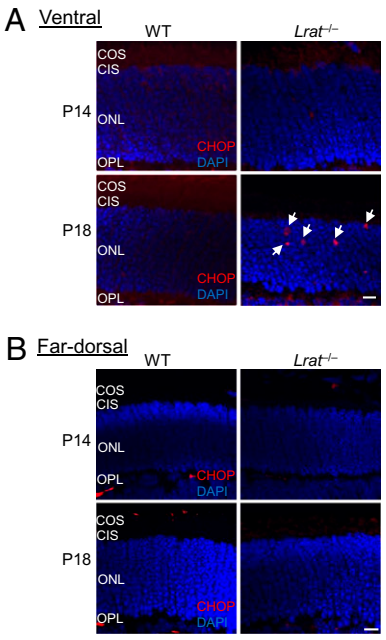

Fig. 4. CHOP activation in the ventral retina of *Lrat*$^{-/-}$ mice. The ventral (*A*) and far dorsal (*B*) retinal sections of WT and *Lrat*$^{-/-}$ mice (P14 and P18) were labeled with a CHOP antibody (red) and DAPI (blue). White arrows indicate CHOP signals in the ONL of the ventral retina of P18 *Lrat*$^{-/-}$ mice. Red signals in the OPL were caused by the labeling of retinal vessels by the Cy3-conjugated goat anti-mouse secondary antibody. (Scale bar: 10 μm.)

a cell culture system (COS-7) in which both rod and cone opsins formed functional pigments after reconstitution with chromophore (19, 20), and in which the aggregation behavior of several proteins causing neurodegeneration in the brain were studied (e.g., ref. 21). We transfected COS-7 cells with plasmids encoding various opsins and HA-tagged ubiquitin. In contrast to the uniform membrane localization of rhodopsin (*SI Appendix*, Fig. S3), all cone opsins showed predominant intracellular distribution (with a "net" structure) when expressed in COS-7 cells (Fig. 5). This is consistent with in vivo observation that cone opsin but not rhodopsin requires 11-*cis*-retinal for the correct trafficking to the outer segment (equivalent to COS-7 cell membrane) of mouse photoreceptors (8–11). Particularly, both mouse S-opsin and human blue opsin showed prominent aggregations manifesting as green dots of varying sizes in the perinuclear region (Fig. 5). This was not observed for mouse M-opsin and human red/green opsins. The intracellular accumulation of both mouse S-opsin and human blue opsin was noticeably higher than that of mouse M-opsin and human red/green opsins, even though the same amount of plasmid was used for transfection. These results resemble the in vivo findings on mouse M and S opsins in the P18 *Lrat*$^{-/-}$ retina (Figs. 1 and 2*A*). In addition, aggregated mouse S-opsin and human blue opsin colocalized with ubiquitin (i.e., ubiquitin exhibited the same aggregated distribution; Fig. 5), which was similar to what we found for S-opsin in P18 *Lrat*$^{-/-}$ cones (Fig. 3*A*). In cells transfected with human red/green and mouse M-opsin, ubiquitin showed weak diffused pattern and poor colocalization with cone opsins (Fig. 5, *Middle*, *Right*). In cells transfected with the vector control, we did not detect any nonspecific signals when using antibodies against various opsins or the HA tag (*SI Appendix*, Fig. S4).

To examine the possibility that the aggregation of short-wavelength opsins may induce UPR and ER stress, COS-7 cells were cotransfected with various opsins and a CHOP-GFP reporter plasmid, which can track the expression of the endogenous CHOP (22). In cells transfected with the vector, there was some basal CHOP-GFP signal (*SI Appendix*, Fig. S5 and Fig. 6). The expression of mouse S and human blue opsins induced significant CHOP activation compared with the expression of rhodopsin, mouse M-opsin or human red/green opsins ($P < 0.001$; *SI Appendix*, Fig. S5 and Fig. 6). This result is consistent with our in vivo observation on CHOP activation in the *Lrat*$^{-/-}$ retina (Fig. 4).

Replacing Rhodopsin with S-Opsin in *Lrat*$^{-/-}$ Rods Caused Rapid Rod Degeneration. Rods and cones share similarities in the synthesis and transport of visual pigments. For example, cone pigment expressed transgenically in rods targeted correctly to ROS (23–26) and rhodopsin transgenically expressed in cones targeted to the cone outer segment (24). We reasoned that if we replaced rhodopsin with S-opsin in *Lrat*$^{-/-}$ rods, S-opsin would likely mistraffic and accelerate rod degeneration. We therefore bred an existing mouse line, *S-opsin*$^{+}$, which expresses S-opsin in rods (26), with rhodopsin KO mice (*Rho*$^{-/-}$) to obtain *S-opsin*$^{+}$*Rho*$^{-/-}$, and then bred *S-opsin*$^{+}$*Rho*$^{-/-}$ with *Lrat*$^{-/-}$ to obtain *S-opsin*$^{+}$*Rho*$^{-/-}$*Lrat*$^{-/-}$ mice. As shown previously, S-opsin in *S-opsin*$^{+}$*Rho*$^{-/-}$ rods can substitute rhodopsin to form a ROS, although it is shorter because of the lower expression level of S-opsin (~6.3% of rhodopsin in WT retina) (26) (Fig. 7*A*, *Left*, red signal). However, in *S-opsin*$^{+}$*Rho*$^{-/-}$*Lrat*$^{-/-}$ rods lacking 11-*cis*-retinal, S-opsin was mislocalized to the rod inner segment, ONL, and OPL layers (Fig. 7*A*, *Middle*). S-opsin aggregates can be seen in the inner segment (Fig. 7*A*, *Right*, white arrows). These features are very similar to those in *Lrat*$^{-/-}$ cones.

Compared with *S-opsin*$^{+}$*Rho*$^{-/-}$ (or *S-opsin*$^{+}$*Rho*$^{-/-}$*Lrat*$^{+/-}$) mice, *S-opsin*$^{+}$*Rho*$^{-/-}$*Lrat*$^{-/-}$ mice exhibited rapid rod degeneration irrespective of retinal regions (Fig. 7 *C* and *D*). This is in sharp contrast to the cone degeneration pattern in *Lrat*$^{-/-}$ mice (Fig. 2*C*), suggesting that the slow dorsal *Lrat*$^{-/-}$ cone degeneration is not a result of region-specific factors (e.g., more residual chromophore in the dorsal retina). The ONL thickness of *S-opsin*$^{+}$*Rho*$^{-/-}$*Lrat*$^{-/-}$ mice was slightly reduced at P14, and

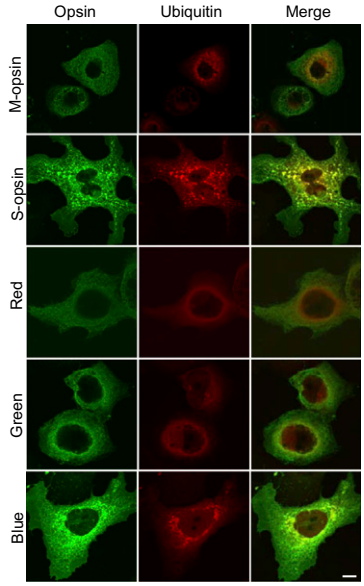

Fig. 5. Aggregation and ubiquitination of mouse S-opsin and human blue opsin in COS-7 cells. COS-7 cells were cotransfected with various opsin-encoding plasmids and an HA-tagged ubiquitin plasmid (*Materials and Methods*). Transfected cells were double-labeled with antibodies against the HA tag and various opsins. Both mouse S-opsin and human blue opsin formed intracellular aggregates (green dots). (Scale bar: 10 μm.)

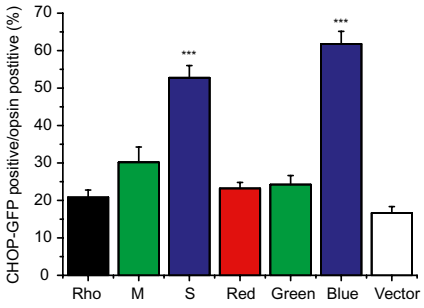

Fig. 6. Quantification of CHOP-GFP–positive cells as percentages of opsin-expressing cells. COS-7 cells were cotransfected with plasmids encoding CHOP-GFP and various opsins (or control vector pRK5 and pmCherry-N1), and were labeled with opsin antibodies. The numbers of vector-transfected cells were estimated from mCherry-positive cell. $N = 10$ for Rho; $n = 11$ for M, red, blue; $n = 12$ for S and green opsins; $n = 6$ for vector control. Both mouse S-opsin (S) and human blue opsin induced significantly more CHOP activation than mouse M-opsin (M), human red/green opsins, bovine rhodopsin, and vector control. $^{***}P < 0.001$.

was drastically reduced (~50%) at P21. This degeneration rate was faster than that of ventral/central cone degeneration in $Lrat^{-/-}$ and $Rpe65^{-/-}$ (8–11) (Fig. 2*C*). Thus, replacing rhodopsin with S-opsin in $Lrat^{-/-}$ rods accelerated the rod degeneration dramatically. Aggregated S-opsin induced marked CHOP activation in P14 *S-opsin*$^{+}$*Rho*$^{-/-}$*Lrat*$^{-/-}$ retina compared with the control *S-opsin*$^{+}$*Rho*$^{-/-}$ retina (Fig. 7*B*). The CHOP signal was unlikely from cones, because P14 $Rho^{-/-}Lrat^{-/-}$ retina showed no CHOP activation (*SI Appendix*, Fig. S6), similarly as seen in the P14 $Lrat^{-/-}$ retina (Fig. 4). Moreover, *S-opsin*$^{+}$$Rho^{-/-}Lrat^{-/-}$ rods degenerated much faster than $Rho^{-/-}Lrat^{-/-}$ rods (*SI Appendix*, Fig. S7), suggesting that the degeneration is mainly caused by toxic accumulation of mistrafficked S-opsin in the inner segments, ONL, and synaptic regions of rods rather than insufficient delivery of opsins into ROS.

Discussion

The outer segments of rods and cones are renewed approximately every 10 d in higher vertebrates (27, 28). New discs are assembled at the base of the outer segments and old discs are ingested at the tip by neighboring RPE. During this process, membrane proteins like rod and cone opsins are synthesized in the inner segment, targeted to the outer segment, and eventually degraded by RPE via phagocytosis. In the $Lrat^{-/-}$ model, large quantities of M and S opsins are mislocalized to the inner regions of cones, creating an extra burden on the cell. However, the two types of cone opsins face very different fates in cones: a significant amount of mislocalized M-opsin was degraded, whereas S-opsin was resistant to proteasome degradation, resulting in far more toxic aggregation of S-opsin in the ventral and central retina than of M-opsin in the dorsal retina. In addition, we demonstrated that the aggregation of S-opsin led to CHOP activation. It is likely that the UPR in cones copes with mislocalized M-opsin more effectively than mislocalized S-opsin. Thus, M-opsin is degraded by the ER-associated degradation pathway, which relieves ER stress. To the contrary, S-opsin is resistant to ER-associated degradation, resulting in aggregation/accumulation, which induces apoptosis. Our results explain the region-specific cone degeneration pattern in $Lrat^{-/-}$ and $Rpe65^{-/-}$ retinas. In earlier immunostaining studies on $Rpe65^{-/-}$ and $Lrat^{-/-}$ retinas (8, 11), S-opsin was hardly detectable because the AB5407 antibody did not recognize S-opsin apoprotein (i.e., without chromophore) (*SI Appendix*, Fig. S8). In contrast, the MBO antibody (26) we used in this study can detect both chromophore-bound and chromophore-free S-opsin on immunohistochemistry (*SI Appendix*, Fig. S8).

To our knowledge, this is the first demonstration that cone opsins have distinct aggregation properties in the absence of 11-*cis*-retinal. By analyzing the aggregation propensity profile with Zyggregator, a computer algorithm that identifies aggregation-prone regions of a misfolded protein based on the hydrophobic pattern, secondary structure propensity, and charges of amino acid sequences (29), we found that a region formed by residues 70 to 125 in S-opsin (72–127 in human blue) has a high probability to aggregate (*SI Appendix*, Fig. S9, boxed areas; intrinsic aggregation score $Z_{agg} > 1.0$). Human red/green opsins and mouse M-opsin do not have such a concentrated aggregation region. Close inspection of this region (including helix II, extracellular loop I, and helix III) revealed that there are nine phenylalanine residues in the S-opsin and human blue, whereas there is only one in human red/green and M-opsin (Fig. 8, underlined). This may explain why the short-wavelength opsins are more susceptible to aggregation in the absence of 11-*cis*-retinal because aromatic residues (particularly phenylalanine), play a significant role in the aggregation of proteins with folding defects by directing molecular recognition and self-assembly via π–π interactions (30). Based on this analysis, we predict that the aggregation-prone property is a common feature of the vertebrate short-wavelength opsins (SW1) because of the conservation of the phenylalanine-rich region in this family (*SI Appendix*, Fig. S10). In contrast, majorities of long and medium-wavelength vertebrate opsins contain one or two phenylalanine residues (except some species of fish have four; *SI Appendix*, Fig. S11), suggesting that vertebrate L/M opsins are less likely to aggregate and are more susceptible to proteasome degradation in the absence of 11-*cis*-retinal.

Previous works suggest that the short-wavelength pigments are thermally much more stable than the long-wavelength pigments (actually with thermal stability more similar to rhodopsin) (31, 32). It is likely that the phenylalanine-rich region may play a dual role for the SW1 opsins. When the opsin is folded correctly in the presence of 11-*cis*-retinal, it promotes protein stability. Conversely, when the opsin is folded incorrectly without 11-*cis*-retinal,

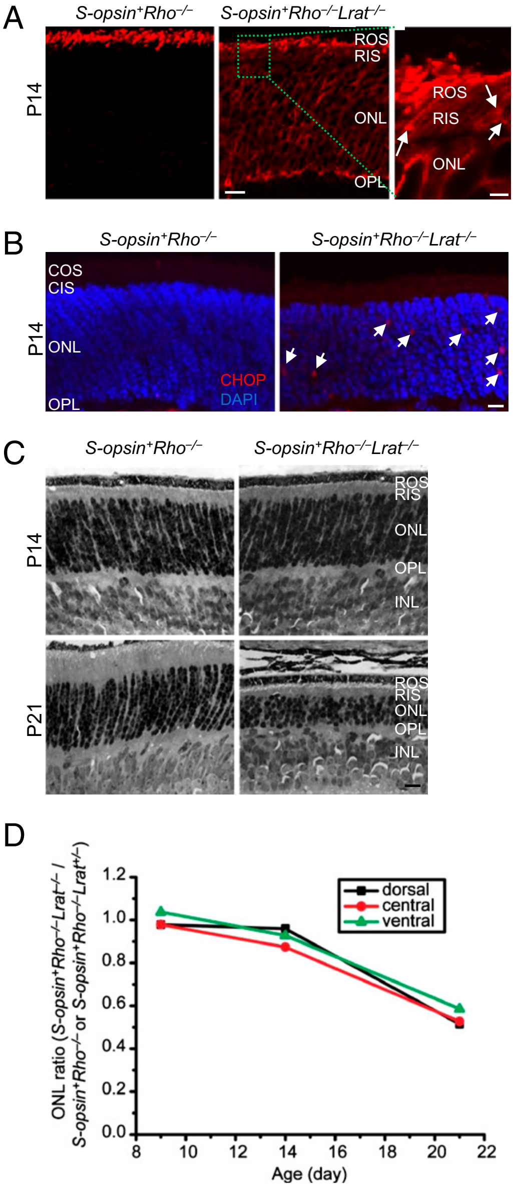

Fig. 7. Replacing rhodopsin with S-opsin in $Lrat^{-/-}$ rods caused rapid rod degeneration. (*A*) Mistrafficking of S-opsin in *S-opsin*$^{+}$*Rho*$^{-/-}$*Lrat*$^{-/-}$ rods. P14 *S-opsin*$^{+}$*Rho*$^{-/-}$ and *S-opsin*$^{+}$*Rho*$^{-/-}$*Lrat*$^{-/-}$ retinal sections were immunostained for S-opsin (red). Aggregation of S-opsin in the inner segment of *S-opsin*$^{+}$*Rho*$^{-/-}$*Lrat*$^{-/-}$ rods is indicated by white arrows in the magnified view of a boxed region. (*B*) CHOP activation in the *S-opsin*$^{+}$*Rho*$^{-/-}$*Lrat*$^{-/-}$ retina. The retinal sections of P14 *S-opsin*$^{+}$*Rho*$^{-/-}$ and *S-opsin*$^{+}$*Rho*$^{-/-}$*Lrat*$^{-/-}$ mice were labeled with a CHOP antibody (red) and DAPI (blue). White arrows indicate CHOP signals in the ONL of the *S-opsin*$^{+}$*Rho*$^{-/-}$*Lrat*$^{-/-}$ retina. Immunolabeling with an isotype control antibody for CHOP did not show nonspecific signals (*SI Appendix*, Fig. S13). (*C*) Comparison of rod degeneration in *S-opsin*$^{+}$*Rho*$^{-/-}$*Lrat*$^{-/-}$ and *S-opsin*$^{+}$*Rho*$^{-/-}$ mice at the indicated ages. Retinas were embedded in plastic, and 1-μm cross-sections were stained by hematoxylin and eosin. INL, inner nuclear layer. (*D*) The average ONL length at the ventral, central, and dorsal retina of *S-opsin*$^{+}$*Rho*$^{-/-}$*Lrat*$^{-/-}$ mice at P9, P14, and P21 were normalized against those of control *S-opsin*$^{+}$*Rho*$^{-/-}$ or *S-opsin*$^{+}$*Rho*$^{-/-}$*Lra*$^{+/-}$ mice (*Materials and Methods*). (Scale bars: *A*, *Right*, 2 μm; *A*, *Left*, *Middle*, 10 μm; *B*, 5 μm; *C*, 10 μm.)

it promotes aggregation. Interestingly, the same region in rhodopsin contains seven phenylalanine residues (Fig. 8), which may be partly responsible for rhodopsin's thermal stability. This region does not promote aggregation of WT rhodopsin because rhodopsin folds correctly and traffics to ROS without 11-*cis*-retinal (8, 11). Thus, 11-*cis*-retinal is essential not only for light detection, but also for preserving a transport-competent conformation of cone opsins and preventing aggregate formation, which is achieved by shielding hydrophobic surfaces (e.g., 70–125 in S-opsin) from forming inappropriate intra- or intermolecular contacts during protein synthesis and transport (i.e., as a chemical chaperone).

```
                     H-II
S-opsin  70 ILVNVSLGGFLFCIFSVFTVFIASCHGY 97
Blue     72 ILVNVSFGGFLLCIFSVFPVFVASCNGY 99
Red      91 ILVNLAVADLAETVIASTISIVNQVSGY 118
Green    91 ILVNLAVADLAETVIASTISVVNQVYGY 118
M-opsin  86 ILVNLAVADLAETIIASTISVVNQIYGY 113
Rho      78 ILLNLAVADLFMVFGGFTTTLYTSLHGY 105

           E-I          H-III
S-opsin  98 FLFGRHVCALEAFLGSVAGLVTGWSLAF 125
Blue    100 FVFGRHVCALEGFLGTVAGLVTGWSLAF 127
Red     119 FVLGHPMCVLEGYTVSLCGITGLWSLAI 146
Green   119 FVLGHPMCVLEGYTVSLCGITGLWSLAI 146
M-opsin 114 FVLGHPLCVIEGYIVSLCGITGLWSLAI 141
Rho     106 FVFGPTGCNLEGFFATLGGEIALWSLVV 133
```

Fig. 8. The aggregation-prone regions of S-opsin and human blue identified by Zyggregator are enriched with phenylalanine. Regions in M-opsin, human red/green, and bovine rhodopsin that are homologous to residues 70 to 125 of S-opsin (72–127 of human blue) are aligned. Phenylalanine residues are underlined. The secondary structures of cone opsins are modeled from the rhodopsin crystal structure (39).

In $Lrat^{-/-}$ mouse, rod opsin traffics normally to ROS (7, 8) whereas cone opsins accumulated in inner regions of cones (8–11). This leads to very different consequences on the survival of rods and cones. Rods degenerate slowly because of the constitutive activity of rod opsin (12), whereas cones degenerate rapidly because of the accumulation of mislocalized cone opsins. Nevertheless, there is one feature in common between the two systems: opsin plays a major role in determining the degeneration rate for both rods and cones under 11-*cis*-retinal deprivation. As cone opsins from the same family have similar aggregation and accumulation propensity when 11-*cis*-retinal is limited (Fig. 5), we propose that, in patients with LCA, blue cones die first as a result of toxic accumulation of blue opsin, which is followed by red/green cones dying with less accumulation of mislocalized red/green opsins. The different degeneration rate of different types of cones caused by cone opsins has implications in designing therapeutic approaches. Recently, there has been significant progress in treating patients with *RPE65*-LCA with AAV2-mediated gene replacement therapy (33–36). However, successful gene therapy must be performed in young patients who have not yet developed significant retinal degeneration (36, 37). Chemical chaperones that can reduce the accumulation of mislocalized cone opsins have the potential to work synergistically with the current gene replacement therapy by significantly expanding the therapeutic window.

Materials and Methods

Mice. $Lrat^{-/-}$, $Lrat^{+/-}$, *S-opsin*$^{+}$, and $Rho^{-/-}$ mice were generated previously (7, 26, 38). *S-opsin*$^{+}$*Rho*$^{-/-}$ mice were produced by crossing the *S-opsin*$^{+}$ and $Rho^{-/-}$ lines. *S-opsin*$^{+}$*Rho*$^{-/-}$*Lrat*$^{-/-}$ and *S-opsin*$^{+}$*Rho*$^{-/-}$*Lrat*$^{+/-}$ were produced by breeding between *S-opsin*$^{+}$*Rho*$^{-/-}$ and $Lrat^{-/-}$ mice. WT (*C57BL/6J*) mice were purchased from Jackson Laboratory. Animals were reared under cyclic light (12 h light/12 h dark). Additional details on materials and methods used in the present study are provided in *SI Appendix*.

ACKNOWLEDGMENTS. We thank M. McCloskey for help in mouse genotyping, A. Jones for assistance in histology experiment, J. Chen for the *S-opsin*$^{+}$ mice and S-opsin antibody, J. Lem for the $Rho^{-/-}$ mice, J. Nathans and D. Oprian for various opsin-encoding plasmids and antibodies against human cone opsins, and R.S. Molday for the 1D4 antibody. We also thank N. Tian for discussions and comments on the manuscript. Y.F. was supported by the Career Development Award from Research to Prevent Blindness (RPB), an unrestricted grant to the Department of Ophthalmology at the University of Utah from RPB, and the Karl Kirchgessner Foundation award

for Vision Research. W.B. was supported by National Institute of Health Grants EY08123, EY019298, and EY014800-039003 (National Eye Institute core grant); a grant from the Foundation Fighting Blindness; and an RPB Senior Investigator award.

1. Ruiz A, et al. (1999) Molecular and biochemical characterization of lecithin retinol acyltransferase. *J Biol Chem* 274:3834–3841.
2. Moiseyev G, Chen Y, Takahashi Y, Wu BX, Ma JX (2005) RPE65 is the isomerohydrolase in the retinoid visual cycle. *Proc Natl Acad Sci USA* 102:12413–12418.
3. Jin M, Li S, Moghrabi WN, Sun H, Travis GH (2005) Rpe65 is the retinoid isomerase in bovine retinal pigment epithelium. *Cell* 122:449–459.
4. Redmond TM, et al. (2005) Mutation of key residues of RPE65 abolishes its enzymatic role as isomerohydrolase in the visual cycle. *Proc Natl Acad Sci USA* 102:13658–13663.
5. den Hollander AI, Roepman R, Koenekoop RK, Cremers FP (2008) Leber congenital amaurosis: Genes, proteins and disease mechanisms. *Prog Retin Eye Res* 27:391–419.
6. Redmond TM, et al. (1998) Rpe65 is necessary for production of 11-cis-vitamin A in the retinal visual cycle. *Nat Genet* 20:344–351.
7. Batten ML, et al. (2004) Lecithin-retinol acyltransferase is essential for accumulation of all-trans-retinyl esters in the eye and in the liver. *J Biol Chem* 279:10422–10432.
8. Fan J, Rohrer B, Frederick JM, Baehr W, Crouch RK (2008) Rpe65-/- and Lrat-/- mice: Comparable models of Leber congenital amaurosis. *Invest Ophthalmol Vis Sci* 49: 2384–2389.
9. Znoiko SL, et al. (2005) Downregulation of cone-specific gene expression and degeneration of cone photoreceptors in the Rpe65-/- mouse at early ages. *Invest Ophthalmol Vis Sci* 46:1473–1479.
10. Rohrer B, et al. (2005) Cone opsin mislocalization in Rpe65-/- mice: A defect that can be corrected by 11-cis retinal. *Invest Ophthalmol Vis Sci* 46:3876–3882.
11. Zhang H, et al. (2008) Trafficking of membrane-associated proteins to cone photoreceptor outer segments requires the chromophore 11-cis-retinal. *J Neurosci* 28: 4008–4014.
12. Woodruff ML, et al. (2003) Spontaneous activity of opsin apoprotein is a cause of Leber congenital amaurosis. *Nat Genet* 35:158–164.
13. Jacobson SG, et al. (2007) Human cone photoreceptor dependence on RPE65 isomerase. *Proc Natl Acad Sci USA* 104:15123–15128.
14. Applebury ML, et al. (2000) The murine cone photoreceptor: A single cone type expresses both S and M opsins with retinal spatial patterning. *Neuron* 27:513–523.
15. Lehman NL (2009) The ubiquitin proteasome system in neuropathology. *Acta Neuropathol* 118:329–347.
16. Forman MS, Trojanowski JQ, Lee VM (2004) Neurodegenerative diseases: A decade of discoveries paves the way for therapeutic breakthroughs. *Nat Med* 10:1055–1063.
17. Yoshida H (2007) ER stress and diseases. *FEBS J* 274:630–658.
18. Awai M, et al. (2006) NMDA-induced retinal injury is mediated by an endoplasmic reticulum stress-related protein, CHOP/GADD153. *J Neurochem* 96:43–52.
19. Oprian DD, Asenjo AB, Lee N, Pelletier SL (1991) Design, chemical synthesis, and expression of genes for the three human color vision pigments. *Biochemistry* 30: 11367–11372.
20. Merbs SL, Nathans J (1992) Absorption spectra of human cone pigments. *Nature* 356: 433–435.
21. Gu WJ, et al. (2003) The C289G and C418R missense mutations cause rapid sequestration of human Parkin into insoluble aggregates. *Neurobiol Dis* 14:357–364.
22. Novoa I, Zeng H, Harding HP, Ron D (2001) Feedback inhibition of the unfolded protein response by GADD34-mediated dephosphorylation of eIF2alpha. *J Cell Biol* 153:1011–1022.
23. Fu Y, Kefalov V, Luo DG, Xue T, Yau KW (2008) Quantal noise from human red cone pigment. *Nat Neurosci* 11:565–571.
24. Kefalov V, Fu Y, Marsh-Armstrong N, Yau KW (2003) Role of visual pigment properties in rod and cone phototransduction. *Nature* 425:526–531.
25. Sakurai K, et al. (2007) Physiological properties of rod photoreceptor cells in green-sensitive cone pigment knock-in mice. *J Gen Physiol* 130:21–40.
26. Shi G, Yau KW, Chen J, Kefalov VJ (2007) Signaling properties of a short-wave cone visual pigment and its role in phototransduction. *J Neurosci* 27:10084–10093.
27. Young RW (1967) The renewal of photoreceptor cell outer segments. *J Cell Biol* 33: 61–72.
28. LaVail MM (1976) Rod outer segment disk shedding in rat retina: Relationship to cyclic lighting. *Science* 194:1071–1074.
29. Pawar AP, et al. (2005) Prediction of "aggregation-prone" and "aggregation-susceptible" regions in proteins associated with neurodegenerative diseases. *J Mol Biol* 350:379–392.
30. Azriel R, Gazit E (2001) Analysis of the minimal amyloid-forming fragment of the islet amyloid polypeptide. An experimental support for the key role of the phenylalanine residue in amyloid formation. *J Biol Chem* 276:34156–34161.
31. Rieke F, Baylor DA (2000) Origin and functional impact of dark noise in retinal cones. *Neuron* 26:181–186.
32. Ma J, et al. (2001) A visual pigment expressed in both rod and cone photoreceptors. *Neuron* 32:451–461.
33. Bainbridge JW, et al. (2008) Effect of gene therapy on visual function in Leber's congenital amaurosis. *N Engl J Med* 358:2231–2239.
34. Maguire AM, et al. (2008) Safety and efficacy of gene transfer for Leber's congenital amaurosis. *N Engl J Med* 358:2240–2248.
35. Hauswirth WW, et al. (2008) Treatment of Leber congenital amaurosis due to RPE65 mutations by ocular subretinal injection of adeno-associated virus gene vector: Short-term results of a phase I trial. *Hum Gene Ther* 19:979–990.
36. Cideciyan AV, et al. (2008) Human gene therapy for RPE65 isomerase deficiency activates the retinoid cycle of vision but with slow rod kinetics. *Proc Natl Acad Sci USA* 105:15112–15117.
37. Maguire AM, et al. (2009) Age-dependent effects of RPE65 gene therapy for Leber's congenital amaurosis: A phase 1 dose-escalation trial. *Lancet* 374:1597–1605.
38. Lem J, et al. (1999) Morphological, physiological, and biochemical changes in rhodopsin knockout mice. *Proc Natl Acad Sci USA* 96:736–741.
39. Stenkamp RE, Filipek S, Driessen CA, Teller DC, Palczewski K (2002) Crystal structure of rhodopsin: a template for cone visual pigments and other G protein-coupled receptors. *Biochim Biophys Acta* 1565:168–182.